

Evaluation of Reverse Monte Carlo Models based on Molecular Dynamics Simulations: A Case Study of Ion Conducting Network Glasses

Christian R. Müller,¹ Vindu Kathriarachchi,² Michael Schuch,¹ Philipp Maass,³ and Valeri G. Petkov²

¹*Institut für Physik, Technische Universität Ilmenau, 98684 Ilmenau, Germany*

²*Department of Physics, Central Michigan University, Mount Pleasant, Michigan 48859, USA*

³*Fachbereich Physik, Universität Osnabrück, Barbarastr. 7, 49069 Osnabrück, Germany**

(Dated: December 23, 2018)

We investigate the quality of structural models generated by the Reverse Monte Carlo (RMC) method in a typical application to amorphous systems. To this end we calculate surrogate diffraction data from a Li₂O-SiO₂ molecular dynamics (MD) simulation and use the total scattering function, in addition to minimal pair distances and coordination numbers of silicon (oxygen) to oxygen (silicon) ions, as input for the RMC modeling. Then we compare partial radial distribution functions, coordination numbers, bond angles, and ring sizes predicted by the RMC models with those of the MD system. It is found that partial distributions functions and properties on small lengths scales, as distributions of coordination numbers and bond angles, are well reproduced by the RMC modeling. Properties in the medium-range order regime are, however, not well captured, as is demonstrated by comparison of ring size distributions. Due care therefore has to be exercised when extracting structural features from RMC models in this medium-range order regime. In particular we show that the occurrence of such features can be a mere consequence of the chosen starting configuration.

PACS numbers: 61.43.Bn, 61.43.-j, 61.43.Fs

I. INTRODUCTION

The Reverse Monte Carlo (RMC) method is commonly used to build structure models based on experimental data. Introduced by McGreevy and Pusztai in 1988,¹ it has been spreading fast and is now considered a standard method in analyzing structural data. Advantages of this method are its easy implementation and its wide applicability. It has been used to model various material systems such as crystals, polymers and glasses. In principal any structural data can be used as input for the RMC method, but most modelings focus on using diffraction data obtained from X-ray and/or neutron scattering. In ion conducting glass systems RMC models of the structure of the structure have been created for $x\text{Li}_2\text{S}+(1-x)\text{SiO}_2$ glasses,² $0.7\text{SiO}_2+0.3\text{Na}_2\text{O}$ glass,³ $x\text{Na}_2\text{S}+(1-x)\text{B}_2\text{S}_3$ glasses⁴ and $0.5\text{Li}_2\text{S}+0.5[(1-x)\text{GeS}_2+x\text{GeO}_2]$ glasses⁵ among others.

As pointed out by McGreevy, RMC models are “neither unique nor ‘correct’”, but can aid our understanding of local structure properties and their relation to other physical properties.⁶ Accordingly it is important to qualify RMC models for different material classes and to get insight into the limits of this method. This is becoming a more urgent question now, since in recent RMC studies not only the short range order of various network glasses has been investigated, but also the medium range order. Among those studies are discussions of the rings sizes in vitreous SiO₂ and GeO₂,⁷ a detailed investigations of amorphous GeSe₂,⁸ and a proposal of a structural model for multi-component borosilicate glasses, where partial segregation of silicon and boron rich regions is predicted.⁹ It was also suggested to use such models as basis for further investigation of possible conduction pathways of the mobile ions. In this respect the RMC models have been

employed in connection with geometric constraints and the Bond Valence (BV) analysis^{10,11} (see Ref. 12 for a critical discussion of this procedure).

In this paper we test the RMC method against structural data obtained from a Molecular Dynamics (MD) simulation of a Li₂O-SiO₂ glass. For this purpose we calculate surrogate diffraction data from the simulated MD structures and these surrogate data are used as input for the RMC modeling. For the evaluation of the resulting RMC models we determine how well various properties of the original MD structure are reproduced. Particularly we compare properties such as partial radial distribution functions and ring-size distributions, which are not easily accessible by experiment. Through our evaluation it can be clarified how far one can use the RMC method to gain insight into these properties, and where one has to be cautious to take features of the RMC model for real.

We want to stress that for the testing to be valid, it is not necessary that the MD simulation is a particularly good representation of the real lithium silicate glass. Rather, the MD structure can be seen as a valid glass system in itself. We will show that the RMC models generally compare well with the MD structure, but that one has to take care when analyzing features of the medium-range order regime.

II. MOLECULAR DYNAMICS SIMULATIONS

We perform MD simulations of a lithium silicate glass with the chemical formula Li₂O-SiO₂ using the potential model of J. Habasaki and I. Okada.¹³ The cubic simulation box has a length $L = 50.04 \text{ \AA}$ and contains 11664 atoms (3888 Li, 1944 Si, 5832 O) corresponding to a density of 2.27 g/cm^3 and a number density of

TABLE I: Potential parameters for the MD-simulations (cf. Eq. (1)).

Ion	z	a [Å]	b [Å]	c [Å ³ √kJ/mol]
Li ⁺	0.87	1.0155	0.07321	22.24
Si ⁴⁺	2.40	0.8688	0.03285	47.43
O ²⁻	-1.38	2.0474	0.17566	143.98
$f_0 = 4.186 \text{ kJÅ}^{-1} \text{ mol}^{-1}$		$r_c = 1.3 \text{ Å}$		

$\rho_0 = 0.093 \text{ Å}^{-3}$. Periodic boundary conditions are used. The simulations are performed in the NVE ensemble (micro canonical ensemble where the number N of particles, the volume V of the simulation box, and the total energy E are kept constant). The energy E was adjusted so that the temperature of the system fluctuates around a mean value of 301 K with deviations of 2 K. The systems are equilibrated for about 1 ns and the runs for obtaining data have a duration of 2 ns, using a time step interval of $\Delta t = 1$ fs.

The effective interatomic interactions between two atoms of type i and j at distance r are:

$$U_{ij}(r) = \frac{e^2}{4\pi\epsilon_0} \frac{z_i z_j}{r} + f_0(b_i + b_j) \exp\left(\frac{a_i + a_j - r}{b_i + b_j}\right) - \frac{c_i c_j}{r^6} \quad (1)$$

where the parameters listed in Table I have been optimized¹³ and shown to give good agreement with experimental data^{13,14,15,16}. The interaction potential in Eq. (1) is composed of three terms. The first one in (1) is the Coulomb interaction with effective charge numbers for the species. The second term is a Born-Meyer type potential, which takes the short-range repulsive interactions into account, and the third is a dispersive van-der-Waals interaction. It is only used for interactions involving oxygen.

The system was prepared by putting the atoms on a cubic crystal lattice and assigning to every atom random velocities drawn from a Maxwell-Boltzmann distribution corresponding to a temperature of 2500 K, which is well above the (computer) glass transition temperature of this system. From this liquid state the system is cooled down in several steps with intermediate periods of equilibration. First an NVT run (canonical ensemble, where the number N of particles, the volume V and the temperature T are fixed) of 10 ps at 2500 K is performed, followed by an NVE run of the same duration. After simulating another 20 ps in the NVT ensemble and 10 ps under NVE conditions the temperature is decreased in four subsequent sequences down to 300 K. Each cooling cycle consists of a 10 ps run using a thermostat to decrease the temperature linearly, a 10 ps NVT run at the target temperature, and a 10 ps NVE run to verify that there are no temperature drifts. The configurations at the end of the 300 K cooling cycle are used as starting points for a 800 ps long equilibration run using the NVE

TABLE II: Average bound coherent scattering lengths and atomic form factor for Li, Si, and O.

	Li	Si	O
\bar{b}	-1.9	4.1491	5.803
f	3.005	14.41	8.144

ensemble. The measuring runs are 2 ns long. All MD-simulations were carried out with the LAMMPS software package¹⁷.

The partial and total radial distribution functions $g_{ij}(r)$ and $G^{\text{PDF}}(r)$ as well as the total scattering structure factor $S(Q)$ were calculated according to the PDF-formalism (see 18 for a discussion of different possible definitions of scattering functions). The partial radial distribution functions are given as

$$g_{ij}(r) = \frac{n_{ij}(r)}{4\rho_j\pi r^2 dr} \quad , \quad (2)$$

where $n_{ij}(r)$ is the average number of particles of type j between distances $r - dr/2$ and $r + dr/2$ from a particle of type i , and ρ_j is the mean number density of particles of type j .

The total radial distribution function is calculated by

$$G^{\text{PDF}} = 4\pi r \rho_0 \left[\sum_{i,j=1}^m (w_{ij} g_{ij}) - 1 \right] \quad , \quad (3)$$

where ρ_0 is the total number density of the system, m is the number of particle types, and w_{ij} are weighting factors:

$$w_{ij} = \left(\sum_{i=1}^m c_i \bar{b}_i \right)^{-2} \sum_{i,j=1}^m c_i c_j \bar{b}_i \bar{b}_j \quad . \quad (4)$$

Here $c_i = \rho_i/\rho_0$ are the molar fractions of particles of type i , and \bar{b}_i is their average bound coherent scattering length. In order to calculate X-ray diffraction functions one has to replace the \bar{b}_i with the atomic form factors f_i .

Finally, the total structure factor $S(Q)$ is calculated from $G^{\text{PDF}}(r)$ by

$$Q[S(Q) - 1] = \int_0^\infty G^{\text{PDF}}(r) \sin Qr dr \quad . \quad (5)$$

All data from the MD system was averaged over 11 configurations from the 2 ns measurement run, which are 200 ps apart each. The scattering lengths and atomic form factors used in Eq. 4 were taken from Ref. 19 and Ref. 20, respectively, and are listed in Table II. In the following we take the freedom to speak about these surrogate diffraction data simply as “diffraction data” and ask the reader to keep in mind that the data was not measured but calculated from Eqs. 2 to 5.

III. REVERSE MONTE CARLO MODELING

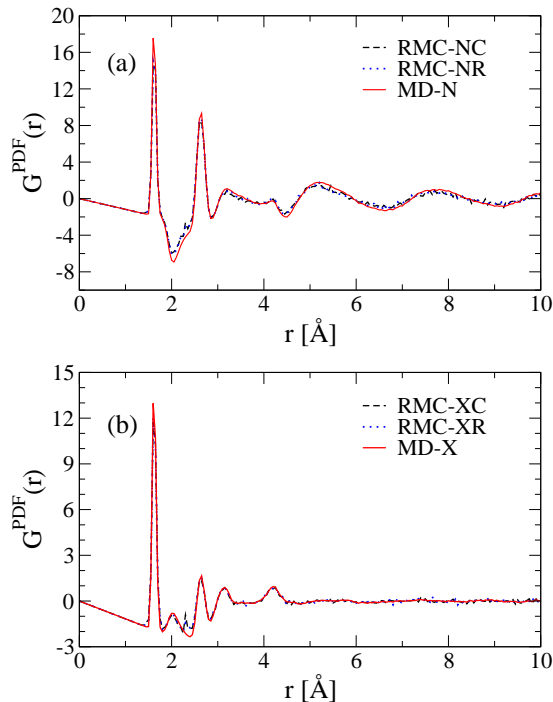


FIG. 1: (color online) Comparison of $G^{\text{PDF}}(r)$ of $\text{Li}_2\text{O-SiO}_2$ RMC models based on crystalline (black dashed line) and random (blue dotted line) starting configurations with that of a $\text{Li}_2\text{O-SiO}_2$ MD system (red solid line). Neutron diffraction data is shown in panel (a) and X-ray diffraction data in panel (b).

RMC simulations were carried out using the RMC++ package.²³ We started with building an initial atomic configuration and then refined it against the $S(Q)$ and $G^{\text{PDF}}(r)$ data computed from the MD structure.

Two starting configurations were considered: a “random distribution” of atoms²⁴ (subsequently referenced by “R”) and another from the $\text{Li}_2\text{O-SiO}_2$ orthorhombic crystal structure (space group Cmc21, subsequently referenced by “C”). Both configurations consists of 3000 atoms (1000 Li, 500 Si, 1500 O). The system was chosen to be cubic with a side length of 31.82 Å so that the atomic number density is the same as in the MD structure. From the random and crystalline starting configurations, two initial models IR and IC were prepared, respectively, by applying the following constraints:

TABLE III: Minimal atomic approach distances as used in the RMC modeling.

Pair	Si-Si	Si-O	Si-Li	O-O	O-Li	Li-Li
r_{\min} in Å	2.8	1.4	2.5	2.3	1.7	2.2

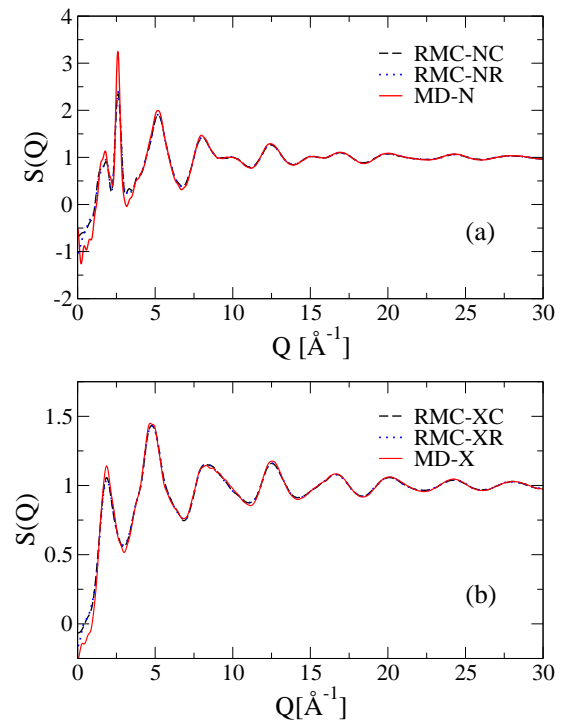


FIG. 2: (color online) Comparison of $S(Q)$ of $\text{Li}_2\text{O-SiO}_2$ RMC models based on crystalline (black dashed line) and random (blue dotted line) starting configurations with that of a $\text{Li}_2\text{O-SiO}_2$ MD system (red solid line). Neutron diffraction data is shown in panel (a) and X-ray diffraction data in panel (b).

- (i) Si is coordinated fourfold with O using a minimal neighbor distance of 1.4 Å and a maximum neighbor distance of 1.8 Å. This corresponds to a 100% fraction $f_{\text{Si,O}}(4) = 1$ of fourfold coordinated Si.
- (ii) The relative numbers of bridging (two Si neighbors) and non-bridging oxygens (one Si neighbor) is 37% and 60%, respectively. This corresponds to $f_{\text{O,Si}}(2) = 0.37$ and $f_{\text{O,Si}}(1) = 0.60$.
- (iii) Minimal atomic distances r_{\min} given in Table III are required.

Intra-tetrahedral O-Si-O angles and inter-tetrahedral Si-O-Si angles were allowed to evolve freely. The preparation was run until the constraints (i)-(iii) were satisfied for at least 95% of the atoms (for given uncertainty parameters, see below).

After creating the initial models, the final refinement is done in order to obtain the best possible agreement be-

TABLE IV: Weighting factors σ_α used for the input quantities in the RMC modeling.

quantity	$S(Q)$	$G^{\text{PDF}}(r)$	$f_{\text{Si,O}}(4)$	$f_{\text{O,Si}}(2)$	$f_{\text{O,Si}}(1)$
σ	10^{-6}	10^{-6}	10^{-4}	$10^{-3,5}$	$10^{-3,5}$

tween the computed $S(Q)$ and $G^{\text{PDF}}(r)$ from the RMC model and the calculated data from the MD-simulation. Both the real space as well as the reciprocal space data was used, since strong low- Q features in $S(Q)$ emphasize the medium range order, while $G^{\text{PDF}}(r)$ shows well defined low- r features which emphasize the short range atomic order. The same constraints as in the preparation of the initial models were applied also during the final RMC modeling.

In the modeling, the input quantities, i.e. the total radial distribution function $G^{\text{PDF}}(r)$, the total structure factor $S(Q)$, and the fractions $f_{\text{Si},\text{O}}(4)$, $f_{\text{O},\text{Si}}(2)$, and $f_{\text{O},\text{Si}}(1)$ of differently coordinated silicon and oxygen ions are taken into account by an effective Hamiltonian of type $H_{\text{eff}} = \sum_{\alpha} \tilde{\chi}_{\alpha}^2 / \sigma_{\alpha}^2$, where $\tilde{\chi}_{\alpha}^2$ is the (unweighted) square deviation between the computed and the measured (in the case of constraints presumed) value of the input quantity α . The weighting factors σ_{α} are summarized in Table IV. For a detailed description of the algorithm we refer to the manual of the RMCA and and RMC++ package which can be downloaded at 25.

In total five RMC models were produced. Two models were generated based on X-ray diffraction data using the random and the crystalline starting configuration (XR model and XC model) and another two are based on the neutron diffraction data (NR model and NC model). A fifth model was generated using both the X-ray and the neutron diffraction data starting from the random configuration (NXR).

In Figs. 1 and 2 the corresponding total structure factors and total distribution functions are compared to the ones calculated from the MD structure. As expected, a good agreement is achieved through the RMC modeling.

IV. COMPARISON OF STRUCTURAL PROPERTIES

A. Partial radial distribution functions

In Fig. 3 partial radial distribution functions $g_{ij}(r)$ (see Eq. 2) are shown. Generally there is a reasonable agreement of the RMC models with the MD structure for Si-Si, Si-O, and Li-O. For g_{OO} the second peak is lacking or too weakly pronounced in the RMC models. This difference can lead to significant deviations of the RMC structures and the MD structure in the medium-range order regime (see also the discussion in Sec. IV D). While there is no dependence upon the starting configuration (crystalline or random), some differences can be seen between the RMC models based on the neutron diffraction data and those based on the X-ray diffraction data. These are most pronounced in g_{SiLi} and g_{LiLi} . The RMC models for which both the neutron and the diffraction data was used show the best agreement with the MD data.

To summarize the result of the comparison of all RMC

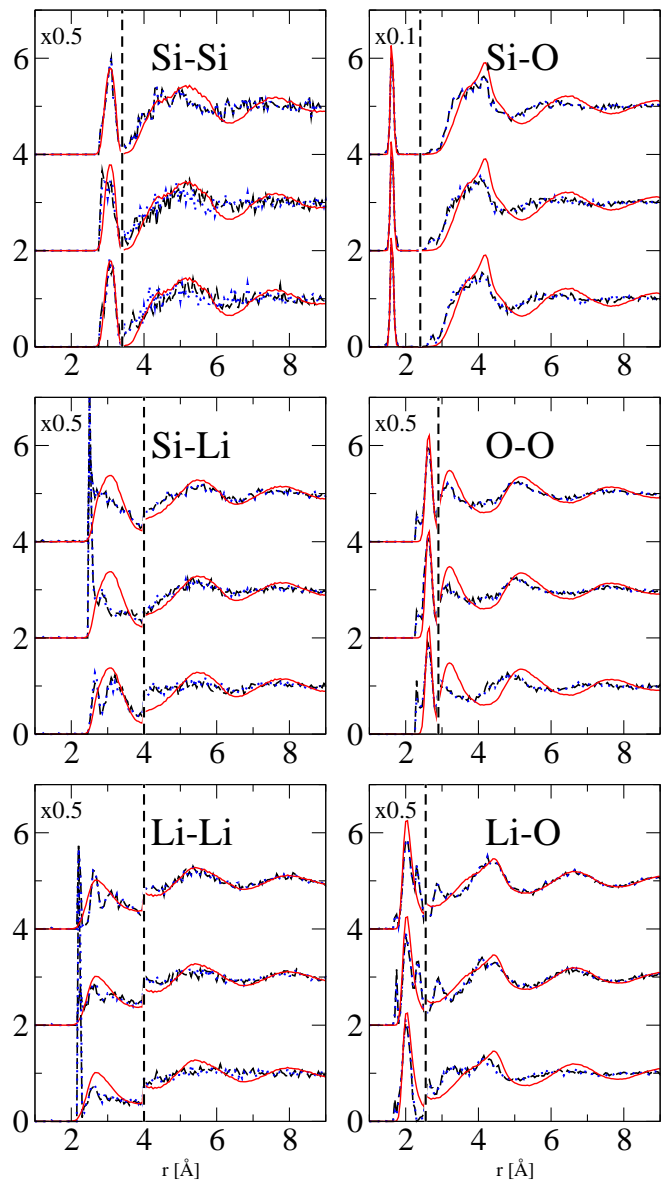


FIG. 3: (color online) Comparison of $g_{ij}(r)$ of $\text{Li}_2\text{O-SiO}_2$ RMC models based on crystalline (black dashed line) and random (blue dotted line) starting configurations with that of a $\text{Li}_2\text{O-SiO}_2$ MD system (red solid line). The RMC model based on neutron diffraction data is shown with a vertical offset of 2, while the RMC model based on both neutron and X-ray diffraction data is shown with an offset of 4. In order to show the full first peak, the curves are scaled by the given factor on the left side of the vertical dashed line in each plot.

models and the MD model, we calculated the integral

$$d_{ij}^{\alpha} = \int |g_{ij}^{\alpha} - g_{ij}^{\text{MD}}| dr \quad (6)$$

over the difference between the partial radial distribution functions of the RMC model α and the MD system. In the numerical calculation we integrated up to $r = 10$, which amounts to an integration to infinity, since $g_{ij}^{\alpha} \cong g_{ij}^{\text{MD}} \cong 1$ for $r \gtrsim 10$. The results shown in Table V

TABLE V: Integrated differences d_{ij}^α of partial radial distribution functions, cf. Eq. (6).

Pair	XC	XR	NC	NR	NXR	IC	IR	C
Si-Si	1.10	1.24	1.42	1.50	1.21	1.56	1.56	9.76
Si-O	1.25	1.29	1.44	1.44	1.28	3.58	3.47	6.58
Si-Li	1.47	1.52	2.36	2.27	1.53	1.63	1.83	9.84
O-O	1.44	1.47	1.03	0.99	0.88	2.29	2.21	5.93
Li-Li	2.03	2.01	1.05	0.97	1.14	1.51	1.58	9.75
Li-O	1.46	1.42	1.24	1.12	0.91	2.01	2.04	6.71
Average	1.46	1.49	1.42	1.38	1.16	2.10	2.12	8.10

allows us to quantify the quality of the RMC models relative to each other. It is surprising that on average the IC and IR models that do not involve information from scattering functions, are not much worse than the RMC models (XC, XR, NC, NR) with only one scattering probe (X-ray or neutron). On the other hand, when information from both scattering probes is taken into account, one obtains a significant improvement on average. We note that this improvement is associated with the fact that the NXR model exhibits good agreement for all individual partial radial distribution functions. By contrast, when the analysis is based on one scattering probe only, quite large deviation can occur for certain partial radial distribution functions (see, for example, $d_{\text{Si,Li}}^{\text{NC}}$ and $d_{\text{Li,Li}}^{\text{XC}}$).

B. Coordination numbers

The first neighbor shell coordination number distributions $f_{ij}(N)$ are defined here as the fractions of atoms of type i which have N atoms of type j within a first neighbor shell radius r_{ij} . Note that being neighbors in the sense of this analysis is not associated with having a chemical bond. To quantify the quality of the various RMC models α , the overlap

$$\phi_{ij}^\alpha = 1 - \sum_{N=0}^{\infty} |f_{ij}^\alpha(N) - f_{ij}^{\text{MD}}(N)|. \quad (7)$$

was calculated. A value $\phi_{ij}^\alpha = 1$ means perfect overlap between the distributions of the coordination numbers $f_{ij}^\alpha(N)$ and $n_{ij}^{\text{MD}}(N)$ of the RMC model α and the MD structure.

The results are summarized in Table VI. No significant differences in the ϕ_{ij}^α are found between the RMC models based on the crystalline starting configuration and the random starting configuration (with one exception for Si-Li, where a larger difference is observed between the RMC-XC and RMC-XR models). This suggests that the quality of reproducing coordination numbers is independent of the starting configuration. A significant difference between the neutron based and the X-ray based RMC models is found in the Li-O coordination numbers,

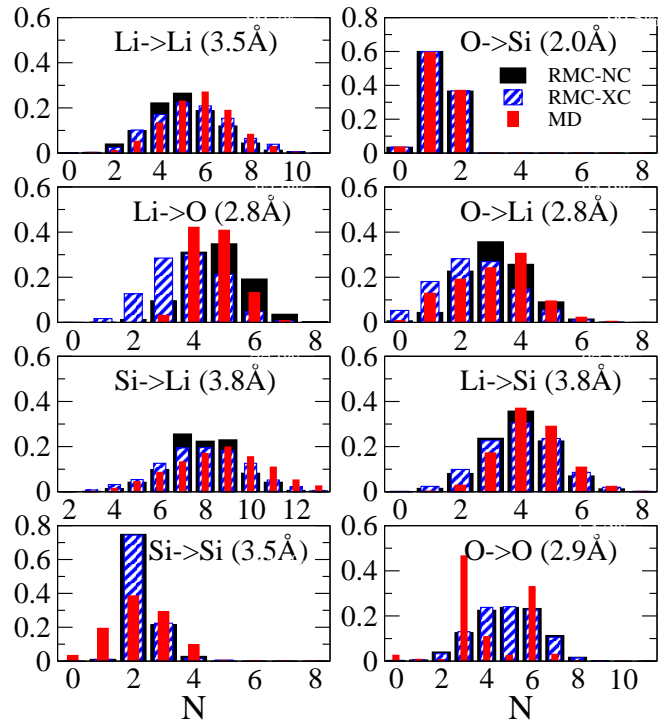


FIG. 4: (color online) Comparison of histograms of coordination numbers of $\text{Li}_2\text{O-SiO}_2$ for RMC models based on a crystalline starting configuration using neutron diffraction data (black solid bars) and X-ray diffraction data (blue striped bars), and the original MD structure (red solid bars). The first atom type is the center atom, and the given distances are the radii of the coordination sphere.

where the better overlap for the neutron based model can be traced back to the higher relative weight of lithium in the neutron diffraction functions. An improved overall agreement is achieved when using both X-ray and neutron diffraction data, though the two most significant discrepancies (Si-Si and O-O) are still there. It is also informative to take a look at the overlap numbers of the initial models that are on the constraints only. These are comparable in quality with the RMC models, which in addition take into account the information from one scattering probe. As for the partial radial distribution functions discussed in the previous Sec. IV A, the RMC-NXR shows a clear improvement compared to the initial RMC models IC and IR.

Figure 4 shows a detailed comparison of the coordination number distributions of the RMC-NC and RMC-XC models with the MD model. For the distribution $f_{\text{SiO}}(N)$ not shown in Fig. 4, we obtained a very good agreement which essentially results from the constraint that silicon atoms must have 4-fold coordination. The most striking discrepancies between the RMC models and the MD structure are found in $f_{\text{OO}}(N)$ and $f_{\text{SiSi}}(N)$. The MD model shows a clear bimodal distribution with maxima at 3 and 6 neighbors (corresponding to non-bridging oxygens and bridging oxygens) in $n_{\text{OO}}^{\text{MD}}(N)$, while the RMC

TABLE VI: Overlap of coordination numbers in percent (see Eq. 7); first neighbor shell radii are given in the second column.

Pair	r_{ij} [Å]	XC	XR	NC	NR	NXR	IC	IR	C
Si-O	2.0	98.4	98.8	99.7	98.4	95.4	99.7	98.8	93.2
O-Si	2.0	99.5	99.6	99.5	99.6	99.1	99.6	99.6	91.2
Li-O	2.8	69.8	68.2	83.0	85.1	87.7	69.3	69.8	48.8
O-Li	2.8	84.5	82.5	84.9	84.9	86.6	83.1	84.5	57.6
Si-Li	3.8	90.4	80.9	77.8	78.5	83.8	80.6	74.5	47.7
Li-Si	3.8	89.5	87.9	87.1	86.7	89.2	84.7	81.7	49.0
Si-Si	3.5	64.0	65.1	64.5	61.9	62.3	66.0	64.1	63.9
O-O	2.9	52.9	52.0	54.2	54.3	58.9	51.6	51.1	89.9
Li-Li	3.5	82.4	81.5	79.5	81.2	92.8	84.4	84.9	52.6
Average	–	81.3	79.6	81.1	81.2	84.0	79.9	78.8	66.0

models have a broad smooth distribution. On the other hand, $n_{\text{SiSi}}^{\text{RMC}}(N)$ is much narrower than $n_{\text{SiSi}}^{\text{MD}}(N)$. These findings suggest that the short-range order of the RMC models corresponds quite well to that of the MD structure, but that the medium-range order, and particularly the structure of the Si-O network, has significant differences. We note, that there are virtually no differences between $f_{\text{SiSi}}(N)$ and $f_{\text{OO}}(N)$ among the five RMC models.

In summary we can conclude that most features in the coordination number distribution are already captured by the constraints. This may not be surprising, since coordination numbers for Si and O have been used as input requirements together with the rather high density of the system. As a consequence, there is not much freedom for the coordination numbers between other types of ion pairs.

C. Bond-angle distribution

We calculated bond-angle distributions for intra-tetrahedral angles (O-Si-O) and inter-tetrahedral angles (Si-O-Si) and found that all RMC models have essentially the same bond-angle distributions. Differences lie within the statistical spread.

In Fig. 5 the distributions for the RMC-NR and RMC-XC model are compared to that of the MD structure. The Si-O-Si bond-angle distribution of the RMC models agrees well with the MD data. The intra-tetrahedral bond-angles, on the other hand, are much broader distributed in the RMC models than in the MD structure. This impression can be quantified by calculating the mean angles $\bar{\alpha}(\text{Si-O-Si})$ and $\bar{\alpha}(\text{O-Si-O})$ as well as the standard deviations $\Delta\alpha(\text{Si-O-Si})$ and $\Delta\alpha(\text{O-Si-O})$. It is found that the mean angles of all RMC models agree very well with the MD values, while the standard deviations are larger by a factor of two, see Table VII. This finding corresponds to the deviations observed in the partial radial distribution functions in Fig. 3 and the coordination

TABLE VII: Mean values and standard deviations of bond angles.

	MD	XC	XR	NC	NR	NXR	IC	IR	C
$\bar{\alpha}(\text{Si-O-Si})$	141.2	139.8	140.7	137.4	138.6	140.5	138.0	138.5	125.7
$\Delta\alpha(\text{Si-O-Si})$	13.7	13.1	13.6	14.5	14.5	13.1	14.9	15.5	0.5
$\bar{\alpha}(\text{O-Si-O})$	108.8	108.7	108.7	108.7	108.8	109.0	108.2	108.2	108.9
$\Delta\alpha(\text{O-Si-O})$	5.9	13.1	12.9	12.7	12.4	11.3	15.6	15.9	3.2

number distribution of O-O in Fig. 4. There, distinctive features of the MD data, as the second peak in $g_{\text{OO}}^{\text{MD}}$ and the bimodal distribution in $f_{\text{OO}}^{\text{MD}}$, are not well reproduced by the RMC models.

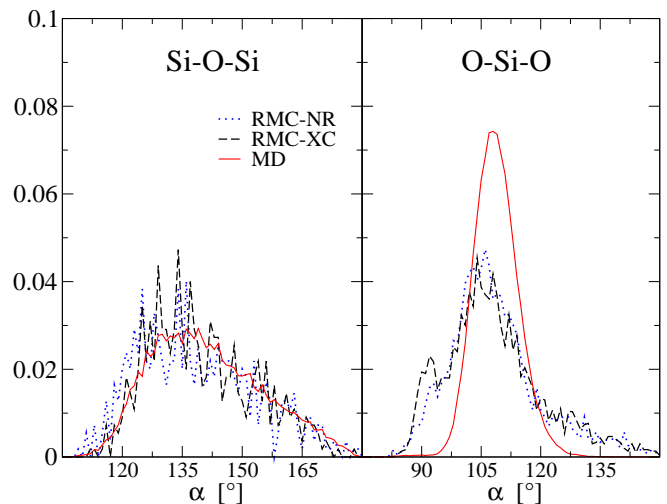


FIG. 5: (color online) Bond-angle distributions of the MD structure (red solid lines) and RMC models based on a crystalline starting configuration using neutron diffraction data (black dashed lines) as well as based on a random starting configuration using X-ray diffraction data (blue dotted lines). In the left panel the distributions of intra-tetrahedral angles (O-Si-O), and in the right panel the distributions of inter-tetrahedral angles (Si-O-Si) are shown.

D. Ring-size distribution

In order to compare the topography of the glass-network we determined ring-size distributions for each model. Here rings and their size are defined in the following manner:

- (i) A Si-atom and an O-atom are considered neighbors if their distance is smaller than 2.0 Å (using closest image convention).
- (ii) For each Si-atom γ , the smallest closed loop of alternating neighboring silicon and oxygen atoms is determined, which entails the Si-atom γ .
- (iii) The size of the ring is equal to the number of its Si-atoms.

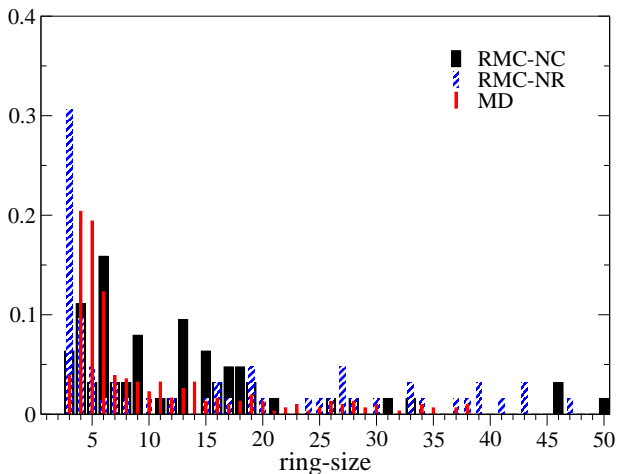


FIG. 6: (color online) Comparison of ring-size distribution of $\text{Li}_2\text{O-SiO}_2$ RMC models based on a crystalline starting configuration using neutron diffraction data (black wide bars) and based on a random starting configuration (blue striped bars) with that of a $\text{Li}_2\text{O-SiO}_2$ MD system (red narrow bars).

The maximum number of rings equals the total number of Si-atoms. However the number of rings is generally smaller, since there are a number of Si-atoms for which no ring is found (e. g., for an isolated SiO_4 tetrahedra), and two different Si-atoms can be associated with the same ring.

In Fig. 6 the ring-size distributions of the MD system, the RMC-NC and the RMC-NR-model are shown. No data is shown for the X-ray and combined data based RMC models, since their ring-size distributions are practically the same as for the neutron diffraction data based RMC models. Indeed the ring-size distributions almost do not change compared to those of the initial models. On the other hand, there is a clear dependence upon the starting configurations. While most rings (40%) of the RMC-NR model are of size three and four, the RMC-NC model has a high number of rings of size 4 and 6. The latter is more in line with what is found in the MD system.

The RMC-NC model has a high number of rings of a size larger than 10. Examining these large rings in more detail reveals that most of them are actually straight linear chains penetrating the system parallel to one system axis (they are seen as rings due to the periodic boundary conditions, and can be found in both the RMC-NC and the RMC-XC models; see also Fig. 7). Such straight chains are not seen in the RMC-NR and the RMC-XR models and in the MD structure. There are also large rings and chains in these models, but those are generally much more twisted than in the RMC models based on the crystalline starting configurations.

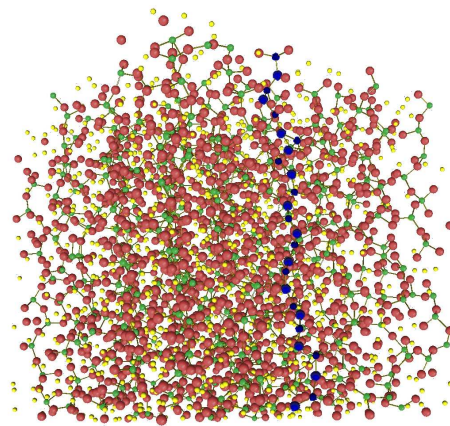


FIG. 7: (color online) Picture of the RMC model based on a crystalline starting configuration. Lithium atoms are marked as small yellow spheres, Silicon atoms as medium sized green spheres, and Oxygen atoms as large red spheres. In the center a linear chain of neighboring Si and O is marked in dark blue, which is a leftover of the starting configuration.

V. SUMMARY AND CONCLUSIONS

The RMC method successfully reproduces many salient features of the local structure of the original MD system. Some differences are found in the partial radial distribution function of O-O, and in the coordination number distributions of Si-Si and O-O. With respect to the structure beyond nearest neighbor distances the RMC models are less predictive and therefore cannot be expected to capture the medium range order properly.

Comparing RMC models based on X-ray and neutron scattering data revealed no significant differences. Moreover, we found that the additional consideration of scattering data from one type of probe (either X-ray or neutron) gives only a modest improvement over the initial RMC models that are based on geometric constraints only (number density, minimal pair distances, some coordination numbers). The situation becomes much better, however, when including the information from both types of scattering probes.

Most structural properties of the RMC models do not depend sensitively on the starting configuration (crystalline or random). Even the ring-size distributions do not differ that much. However, taking a closer look at the rings, revealed that the RMC models based on the crystalline starting configuration exhibit straight linear chains penetrating the system. These straight chains are remnants of the crystalline starting configuration and their occurrence is not reflected in the other structural properties studied. In particular, there are no differences in $G^{\text{PDF}}(r)$ and $S(Q)$ between the RMC models based on the crystalline and the random starting configuration. These findings show that one should check carefully if a

feature of interest in RMC models is only a product of a particular starting configuration or if it can be reproduced using totally different starting configurations.

(DFG Grant number MA 1636/3-1) and by the NSF (NSF DMR Grant number 0710564).

Acknowledgments

Work on this project was supported in the Materials World Network by the Deutsche Forschungsgemeinschaft

-
- * Electronic address: philipp.maass@uni-osnabrueck.de;
URL: <http://www.statphys.uni-osnabrueck.de>
- ¹ R. L. M. Greevy and L. Pusztai, *Mol. Simul.* **1**, 359 (1988).
 - ² H. Uhlig, M. J. Hoffmann, H. P. Lamparter, F. Aldinger, R. Bellissent, and S. Steeb, *J. Am. Ceram. Soc.* **79**, 2839 (1996).
 - ³ M. Fabian, P. Jovari, E. Svab, G. Meszaros, T. Proffen, and E. Veress, *J. Phys.: Condens. Matter* **19**, 335209 (2007).
 - ⁴ W. Yao, S. W. Martin, and V. Petkov, *J. Non-Cryst. Solids* **351**, 1995 (2005).
 - ⁵ D. L. Messurier, V. Petkov, S. W. Martin, Y. Kim, and Y. Ren, *J. Non-Cryst. Solids* **355**, 430 (2009).
 - ⁶ R. L. McGreevy, *J. Phys.: Condens. Matter* **13**, R877 (2001).
 - ⁷ S. Kohara and K. Suzuya, *J. Phys.: Condens. Matter* **17**, S77 (2005).
 - ⁸ Y. Murakami, T. Usuki, S. Kohara, Y. Amo, and Y. Kameda, *J. Non-Cryst. Solids* **353**, 2035 (2007).
 - ⁹ M. Fabian, E. Svab, T. Proffen, and E. Veress, *J. Non-Cryst. Solids* **354**, 3299 (2008).
 - ¹⁰ S. Adams and J. Swenson, *Phys. Rev. Lett.* **84**, 4144 (2000).
 - ¹¹ J. Swenson and S. Adams, *Phys. Rev. Lett.* **90**, 155507 (2003).
 - ¹² C. Müller, E. Zienicke, S. Adams, J. Habasaki, and P. Maass, *Phys. Rev. B* **75**, 014203 (2007).
 - ¹³ J. Habasaki and I. Okada, *Mol. Simul.* **9**, 319 (1992).
 - ¹⁴ J. Habasaki, I. Okada, and Y. Hiwatari, *J. Non-Cryst. Solids* **183**, 12 (1995).
 - ¹⁵ R. Banhatti and A. Heuer, *Phys. Chem. Chem. Phys.* **3**, 5104 (2001).
 - ¹⁶ A. Heuer, M. Kunow, M. Vogel, and R. Banhatti, *Phys. Chem. Chem. Phys.* **4**, 3185 (2002).
 - ¹⁷ S. J. Plimpton, *J. Comp. Phys.* **117**, 1 (1995), <http://lammps.sandia.gov/>.
 - ¹⁸ D. A. Keen, *J. Appl. Cryst.* **34**, 172 (2001).
 - ¹⁹ V. F. Sears, *Neutron News* **3**, 26 (1992), <http://www.ncnr.nist.gov/resources/n-lengths/>.
 - ²⁰ C. T. Chantler, K. Olsen, R. A. Dragoset, J. Chang, A. R. Kishore, S. A. Kotochigova, and D. Zucker, (2005), <http://physics.nist.gov/ffast> [2009, June 2], originally published in Refs. 21,22.
 - ²¹ C. Chantler, *J. Phys. Chem. Ref. Data* **24**, 71 (1995).
 - ²² C. Chantler, *J. Phys. Chem. Ref. Data* **29**, 597 (2000).
 - ²³ G. Evrard and L. Pusztai, *J. Phys.: Condens. Matter* **17**, S1 (2005).
 - ²⁴ This starting configuration does not correspond to a fully random arrangements of the ions, but to a quasi-random sequential setup as described in Sec. 9.8.2. of the manual of the RMCA program, see Ref. 25.
 - ²⁵ RMC++ manual, <http://www.szfki.hu/~nphys/rmc++/docs.html> (June 2009).